Pergamon

Int. J. Solids Structures Vol. 32, No. 1, pp. 1–26, 1995

0020-7683/95 $9.50 + .00

0020-7683(94)00141-3

DYNAMIC ANALYSIS FOR AN EXPLOSIVE TEST AND ESTABLISHMENT OF FRACTURE TOUGHNESS LOCUS FOR HY-100 STEEL

JOSEPH F. ZARZOUR, DAH-WEI YUAN and
MARY JANE KLEINOSKY
Concurrent Technologies Corporation, Johnstown, PA 15904, U.S.A.

(*Received* 12 *November* 1993; *in revised form* 10 *June* 1994)

Abstract—An investigation of the dynamic fracture behavior of a structural element was conducted by using the recently developed two parameter (J, Q) criterion. Within the framework of this methodology, a systematic study on the nature of crack tip fields and the corresponding constraints was performed. Combining rigorous computational schemes and state-of-the-art fracture toughness tests, the results obtained in this work assure the suitability of the approach undertaken in the aforementioned analysis. Also, the fracture envelope predicted by the (J, Q) approach appears to provide a good agreement with actual experimental test data. Finally, the applicability and the appropriateness of the existing fracture mechanics theories are discussed.

1. INTRODUCTION

The effects of macroscopic cracks on the structural integrity of large marine structures have been studied extensively from research and deployment perspectives. It is well known that both material toughness as well as structural response play important roles in determining crack geometries that may be tolerated. High toughness materials are generally desirable because they dissipate more energy via material flow and crack extension and consequently provide significant ductility. Thus, this class of fracture problems are typically nonlinear and require special attention in the analyses. On the other hand, a structure can be depicted using many interacting factors, such as, geometry, size, load level and the resultant stresses and strains. Since the stress required to initiate a crack decreases as the size of the structure increases, it is therefore unreliable to predict the behavior of a prototype structure based on the behavior of laboratory scale specimens subjected to standard testing procedures. In other words, determination of empirically feasible and theoretically acceptable specimen configurations for testing is crucial. Clearly it is a real challenge to develop an approach which takes both material and structural responses into consideration.

Testing procedures required to inspect and evaluate the soundness of large structures were intensively investigated at the Naval Research Laboratory. It was concluded that the fracture process cannot be scaled, and the use of full-scale models is recommended to fully characterize the structural response. However, because of high cost, full thickness models were generally tested instead of full-scale models. Several structural element tests have since been introduced to evaluate the integrity of welded plates and shells used in various structural applications. The most prominent test procedures are the explosion bulge test (EBT) (Ritter and Dixon, 1985; Puzak and Pellini, 1961), the flawed bulge explosion (FBE) (Elliott *et al.*, 1987), the curve sector element (CSE) (Porter *et al.*, 1988; Porter, 1991), and the hull toughness element (HTE) (Sickles *et al.*, 1991; Gifford, 1991; Gifford *et al.*, 1988, 1990). The latter was developed to simulate the opening mode crack initiation by using a relatively simple and inexpensive set-up. The approach duplicates fracture conditions that exist in these structures when subjected to severe explosion attack. Conditions, which are recognized and incorporated into the test arrangement, are element properties and geometry, straining rate, loading and restraining conditions. Finally, it should be emphasized that in all these tests, a pass/fail criterion is usually utilized for qualifying the dynamic fracture resistance.

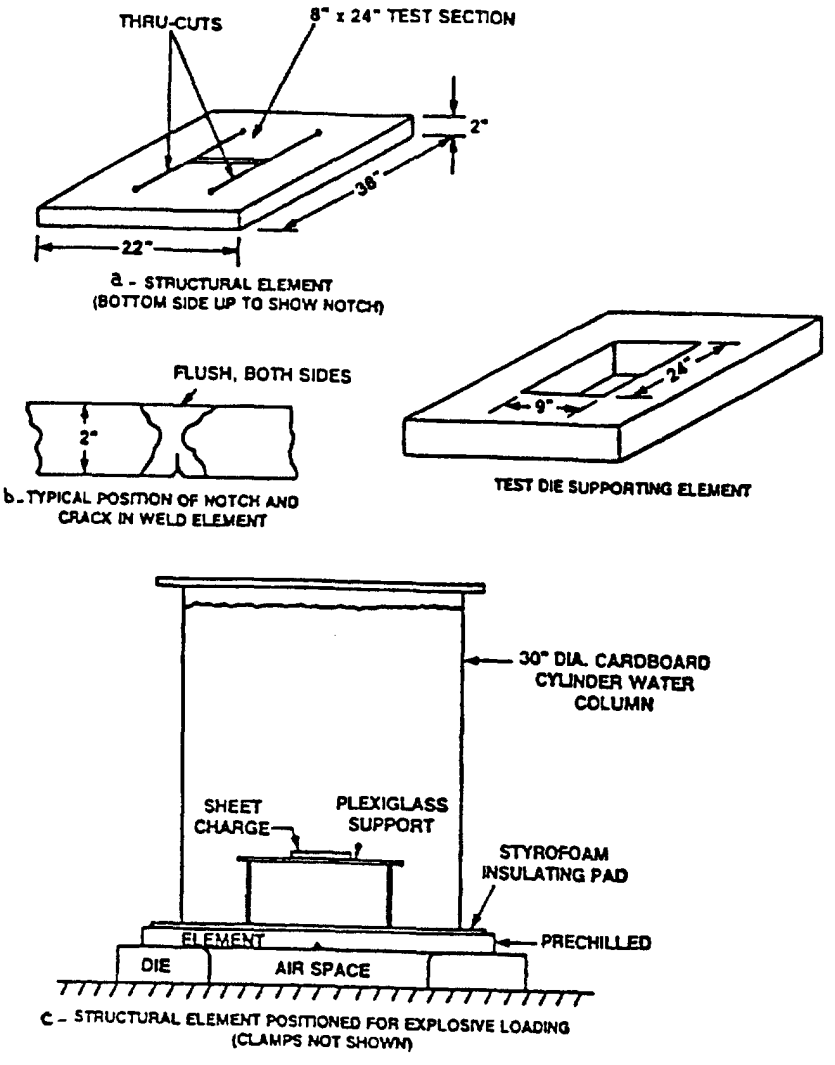

Fig. 1. Experimental setting of the hull toughness element (HTE), after Gifford *et al.* (1990).

The goal of this study is to present a numerical scheme which has been implemented to correlate and interpret the current experimental findings. This approach can also provide a first order prediction of the probability of a crack initiation in the HTEs. Figure 1 shows a schematic of the HTE. It consists of a 2 in thick rectangular plate of dimensions 22 in × 38 in including a test section of 8 in × 24 in located in the central region of the carrier plate [Fig. 1(a)]. They can be fabricated using only a base metal plate or a plate containing weldments. The test section was then formed by cutting two slits in the larger carrier plate. Alternatively, the test section can be welded into a rectangular cavity of any carrier plate of similar material. In either case, a notch which extended across the full 8 in width of the test section was machined on the lower surface and a sharp crack front was subsequently introduced by fatigue [Fig. 1(b)]. The HTE was positioned over a die which served to support the area of the carrier plate that surrounded the test section.

The explosive used to charge the element was immersed in a water column of 30 in diameter and 16–30 in in height. It was placed at a predetermined distance from the structural element as shown in Fig. 1(c). The charge size was selected to produce plastic strains of about 2 to 3% in the upper surface of an uncracked element. Strain gauges were used to record the strain distribution and strain–time histories along the element. As a result, a pressure–time profile, equivalent to the explosive impact sustained by the HTE, was obtained and subsequently used for the finite element analyses (Fig. 2). Explosive tests

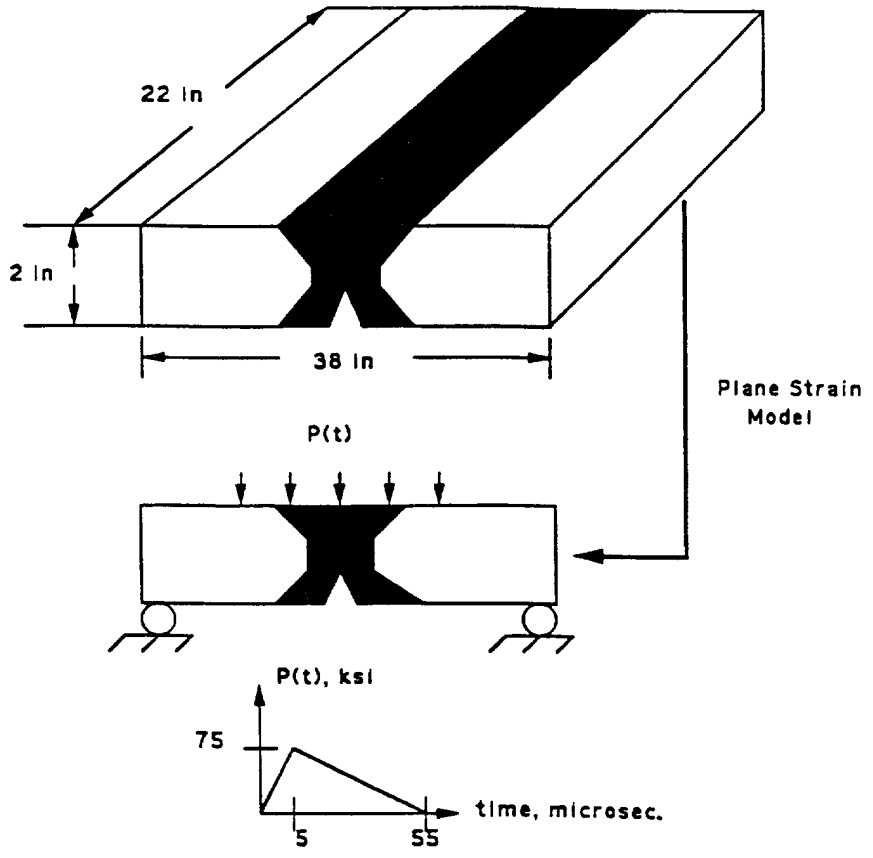

Fig. 2. Actual size, geometry and loading conditions of the HTE.

were also conducted for HTEs containing cracks of various crack length to width ratios ranging from 0.05 to 0.25. It was noted that variables such as the dynamic stress and strain fields developed in the element during the blast are very difficult to qualify because of the violent nature of the test. Therefore, a computational program, which includes finite element analyses of the HTE, was used to characterize the structural response. Figure 3 shows the two finite element models, with and without crack, used in this study to represent the cross sections of the test specimens. These models are analogous to a three point bend test configuration except spring elements were used as end supports to reproduce the actual boundary conditions. It is important to point out that the uncracked model was first examined with an emphasis on closely duplicating the axial strain versus time profile observed in the experiments. Consequently, the boundary conditions established were applied to other HTEs containing surface flaws without further modifications.

2. TECHNICAL APPROACH

The motivation for this study stems from the fact that classical fracture approaches fail to provide a comprehensive solution to the problems involving shallow cracks in high toughness materials. It has been reported that the (J, Q) theory can effectively recognize the stress distribution and the maximum stress achieved ahead of the crack tip under static loading conditions. However, the usefulness of such two parameter fracture mechanics on the dynamic behavior of HTEs is not clear. Therefore, the objective for this investigation is to study whether a (J, Q) fracture criterion can be applied to the cracked HTEs. The efforts involved extensive numerical analyses in conjunction with experimental programs. Determination of the relative instability for cracks of various depths can be achieved. It is conceivable that the success in implementing the (J, Q) methodology to the HTE relies on a reasonable agreement between the numerical prediction and the experimental HTE results.

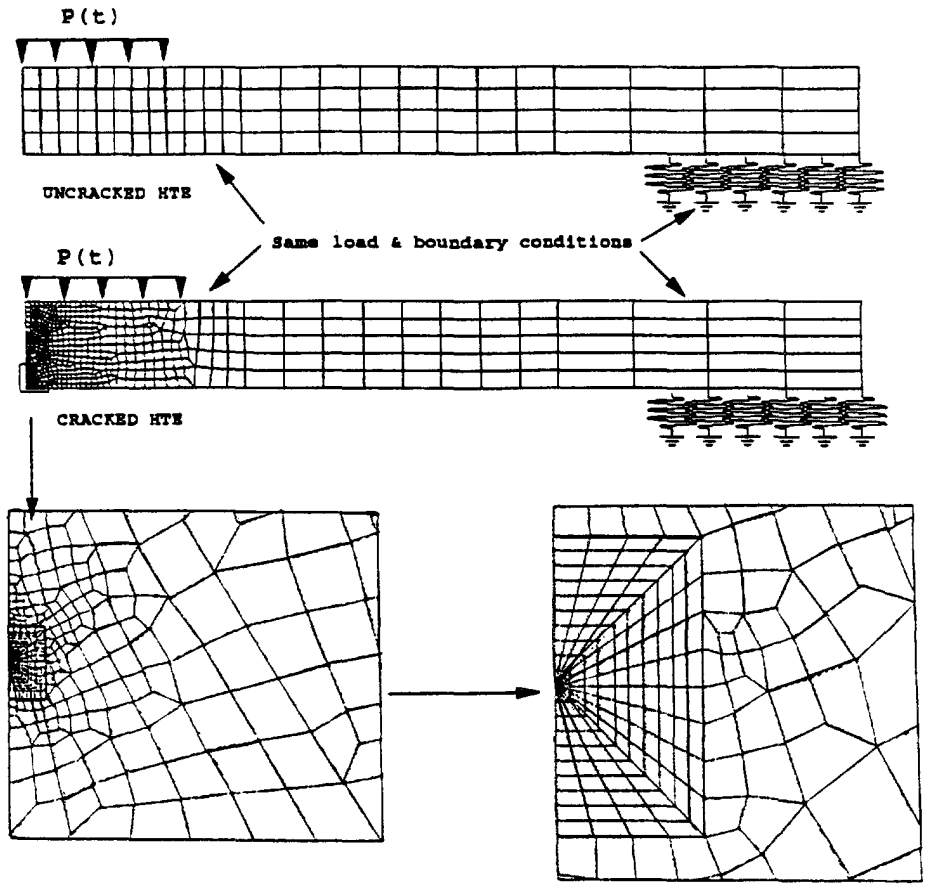

Fig. 3. Finite element mesh for cracked and uncracked HTEs.

Finite element analyses were first pursued to provide detailed information on the structural response under explosive loading conditions. The finite element model without a crack (uncracked HTEs) was carefully constructed and numerically verified so as to reflect and reproduce the actual testing conditions. Analyses were then performed on models which accommodate cracks of various lengths. These models were first subjected to static loads to calculate the baseline properties of single and dual component structures. Furthermore, a load profile representative of the explosive discharge was used to study the dynamic response of the HTEs. The possible influence of induced shock waves on the crack tip stress and strain fields was also examined. Stress gradients near the crack tip regions were analysed according to the two parameter (J, Q) fracture mechanics. Finally, for structures of different properties and crack lengths, trajectories of the typical (J, Q) load paths can be established.

On the other hand, fracture toughness, characterized by the J-integral, for specimens of various crack depths were determined per modified ASTM E813. The corresponding degree of constraint, Q, was calculated based on the initial crack length and the given material properties (O'Dowd and Shih, 1992). The distribution of the resulting J versus Q values was used to delineate the upper and lower bounds of the toughness loci for the material of interest. By superimposing the numerically obtained (J, Q) trajectories, a fracture envelope which defines the load paths leading to an unstable crack growth can be determined. In this paper, the work is organized and presented as follows: (i) selection of material properties; (ii) overall description of the finite element model; (iii) dynamic analyses of cracked and uncracked HTEs with establishment of proper load and boundary conditions; (iv) introduction of the concept of the (J, Q) approach; (v) numerical results; (vi) general discussion followed by a conclusion.

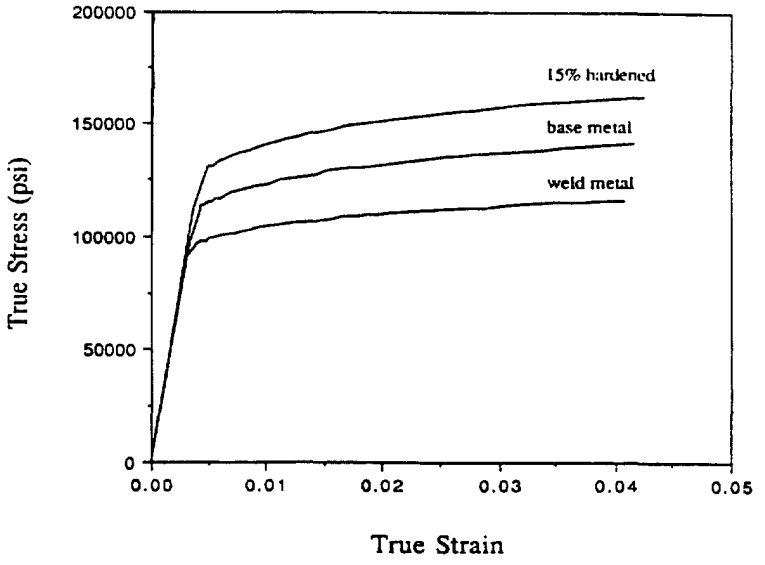

Fig. 4. Different material systems used in the HTE analysis.

3. MATERIAL PROPERTIES

Three different materials were employed in the analysis including base metal (HY-100), weld metal (HY-80), and 15% hardened base metal (HY-115). Results of uniaxial tensile tests conducted at Westmoreland Mechanical Testing and Research Inc. (WMT&R), Youngstown, PA, showed a substantial variability in the stress–strain responses of HY-100 and HY-80 materials. Since dynamic impact is expected to strengthen the materials, those flow curves exhibiting the most hardening behavior are used. In this study, uniaxial yield stresses in tension (σ_0) are 97.2, 89.5 and 111.8 ksi for HY-100, HY-80 and HY-115 steel, respectively. Young's modulus (E) of 30×10^6 psi is used for all the materials. The linear elastic portion of the true stress–true strain curve is characterized by the yield strain (ε_0) of 0.00324 for the HY-100, 0.00298 for the HY-80 and 0.00373 for the HY-115. The corresponding uniaxial true stress–true strain curves used in this study are shown in Fig. 4.

4. FINITE ELEMENT ANALYSES

In order to fully understand the explosive test results, information on the global and local stress and strain state, especially at the crack tip region, is required. For nonlinear elastic–plastic fracture mechanics, the measure of the crack driving force, such as the J-integral, is of equal importance in gaining insight into the local structural response. Unfortunately, within the framework of HTE, it is unlikely to quantify these variables experimentally due to the dynamic nature of the test. Therefore, a computational program consisting of static and dynamic analyses using the finite element scheme is pursued. All the elastic–plastic finite element analyses were performed by using a general purpose finite element code, ABAQUS (1992). These analyses assume a rate-independent J_2 (isotropic hardening) incremental plasticity theory. It is important to note that although ABAQUS is a general purpose finite element code, several dynamic fracture problems have been successfully solved in the literature using ABAQUS [see, for example, Gifford *et al.* (1990); Nakamura (1987); Nakamura *et al.* (1985)]. Moreover, results of some selected benchmark problems with closed-form solutions are also provided in the ABAQUS theory manual. For these reasons, it is presumed that ABAQUS is sufficient for providing dynamic fracture data such as the J-integral versus time with good accuracy.

Static analysis

The goal of this analysis is to establish a baseline computational strategy so that comparison with subsequent dynamic analysis results can be readily obtained. This task

starts with construction of a finite element model that represents the test section of the HTE. A uniform pressure was first applied on the mid-section of the top surface. The numbers and spans of the spring elements used at the end of the structure were varied in order to reproduce the experimentally obtained response. It was determined that springs of constant stiffness ($k = 0.5 \times 10^6$ lb/in/in^2) distributed over a distance of 2.75 in can best describe the actual strain versus time profile (Fig. 3). For static analysis, the immediate focus is to draw a relationship between the crack driving force (J-integral) and the nominal peak strain in the HTE. To achieve this, the peak load required to generate a specific amount of nominal strain of interest must be determined. A static load of 5500 psi was chosen for the HY-100 material to obtain 5% peak strain on both the top and bottom mid-section surfaces. The same load was then applied to HTEs containing various crack lengths so that the corresponding J-integral can be calculated. As a result, the numerical dependence of J-integral on peak strain can be developed without explicitly knowing the applied load.

For cracked HTEs, sizes of elements near the crack tip were chosen to be on the order of the crack tip opening displacement (CTOD). Also, in order to facilitate subsequent analyses, a high mesh density close to the tip is necessary to attain the required resolution in the stress fields. Figure 3 shows a typical finite element model which contains approximately 1200 isoparametric, eight-noded plane strain elements. Because of the symmetry, only half of the HTE was modeled. Sizes of the elements at the first six rings are smaller than 25×10^{-5} in^2. Elastic–plastic finite element analyses were carried out for HTEs with full-width cracks of various depths ($a = 0.05$–0.5 in). The load applied on the cracked element is the same as the one used for the uncracked HTE.

Dynamic analysis

This phase represents the bulk of the effort in the numerical investigation. It includes refinement of the element boundary conditions, the concept of transition time, and the characterization of cracked HTEs by the (J, Q) two parameter approach. The boundary conditions used in the finite element models for the static analyses were modified. The change involves the use of a load history which closely represents the impact due to the explosive charge. A previous study by Gifford *et al.* (1990) indicated that such an explosive impact is capable of producing 2–3% peak nominal strain on the uncracked element and can be approximated by a triangular pressure–time profile. This approximation was derived by the Tailor theory for a plane exponential underwater shock wave (Hilber and Hughes, 1978). The resulting pressure–time history, shown in Fig. 2, consists of a load intensity that increases linearly to a peak pressure of 75 ksi in 5 μs and then decays linearly to zero at 55 μs. The load is distributed uniformly over the top midspan of the element (10 in).

As mentioned in the previous section, plane strain elements are used in the analyses because they are more representative of the crack tip environment. Figure 5(a) shows the resulting axial strain history by using either plane strain or plane stress elements. It is noted that the time to reach peak strain (2.5%) in plane strain conditions provides better resemblance to the actual structural behavior, as shown in Fig. 5(c). These preliminary finite element analyses on the uncracked HTE were performed to bolster confidence in the models and the boundary conditions. They also lay the groundwork to approach the core of the problems where local stress and strain distributions near the crack tips are to be characterized in the cracked elements. However, this cannot be achieved without the knowledge of the structural response due to dynamic stress waves. To that end, material inertia must be considered in the situation involving a stationary crack subjected to a rapidly applied load. As the material at the crack-tip is strained rapidly and, if it is rate sensitive, it offers less resistance to fracture than at quasi-static strain rates. Added to the difficulty of modeling, this behavior implied further changes of material properties due to different strain rates. Materials which undergo a ductile to brittle transition with the lowering of temperature will undergo a similar transition when the loading rate is changed from static to dynamic.

In order to implement the two parameter (J, Q) fracture criterion, local stress and strain fields ahead of the crack tip must be accurately determined. However, concerns over the effects of stress waves on the crack tip region due to a dynamic load at the moment of

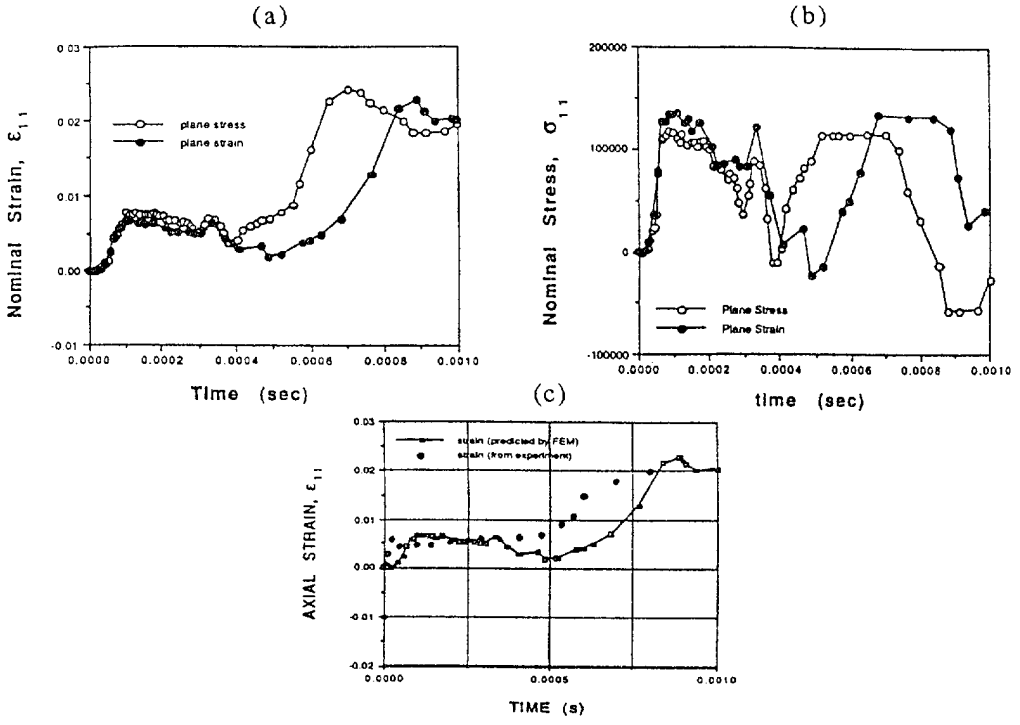

Fig. 5. Nominal stress and strain field in both plane stress and plane strain conditions.

crack initiation must be clarified. It is therefore necessary to closely examine the nature of these fields variables. It is well known that the stress and strain fields at the crack tip are initially dominated by individual stress waves. In the very beginning of an impact test (say three point bend test), stress waves are excited right at the impact point and then propagate within the precracked specimen. The resulting crack loading history is determined by different waves, which interact with the stationary crack directly or after reflection at the boundary. However, the influence of these initial and reflected stress waves at the crack tip starts to diminish as the time increases. Once a transition time τ is reached, a quasi-static loading condition can be applied in the analysis because the impact stress waves are no longer affecting the local stress and strain fields. Since the times-to-fracture for structure under large plastic deformations are fairly long, it would be reasonable to use a quasi-static evaluation procedure in general.

The concept of transition time was first introduced by Nakamura *et al.* (1985) and was examined on several different specimen geometries. The corresponding expression for a three point bend specimen (Nakamura, 1987) is

$$\tau = 23.3\, H/C_0, \tag{1}$$

where H denotes the specimen width and C_0 is the longitudinal wave speed that can be expressed in the following:

$$C_0 = \sqrt{E(1-\nu)/\rho(1+\nu)(1-2\nu)}, \tag{2}$$

where E, ν and ρ are the Young's modulus, Poisson's ratio and mass density of the material, respectively. Based on the material properties of HY-100, the transition time is calculated to be 199.5 μs. In general, the time required for a crack to initiate is about the time when peak strain is approached in the structure. In this analysis the peak strain occurs at about 0.9 ms which is well beyond the transition time. It was then postulated that the effect of inertia on the local stress and strain fields of interest is negligible.

In the analyses of cracked HTEs, small strain theory (up to 10%) with the implicit operator defined by Hilber and Hughes (1978) was used to provide the flexibility of an automatic time stepping scheme and full control over the numerical damping. A default value for the damping parameter $\alpha = -0.05$ was used in order to remove high frequency noise while maintaining the lower frequency response. Also, an option in the ABAQUS code, MPC, was used in the analyses which allows all the nodes at the crack tip to be tied together. This operation effectively reduces the numerical instability and therefore improves the overall efficiency in the computation. Time increments were in the ranges of 10^{-8} to 10^{-4} s. More than 500 time steps were typically required to compute nonlinear response of the structure up to 1 ms. The emphasis of this numerical simulation is to obtain the information on variables required in the interpretation of the (J, Q) fracture criterion, i.e. J-integral and normal stress fields ahead of the crack tip.

5. CONCEPT OF (J, Q) CRITERION

It has been widely observed that the fracture toughness of many classes of steel is geometry dependent (Dodds *et al.*, 1992; Betegon and Hancock 1991; Parks and Wang, 1988). In most cases, specimens loaded in bending give lower J_{Ic} than specimens loaded in tension at an equivalent crack depth. Similarly, shallow cracks give higher J_{Ic} than deep cracks. This geometry dependence is clearly an important issue when related to the crack tip fracture environment. In the past two years, many researchers in the fracture community have advocated the importance of constraint in fracture mechanics. As a result, several new methodologies have emerged and, in particular, the two parameter (J, Q) and (J, T) approaches.

Unlike the one parameter J theory, where J scales the deformation and stress triaxiality at the crack tip, the (J, Q) two parameter approach, proposed by O'Dowd and Shih (1991, 1992), introduced an additional parameter Q which enabled the decoupling of the above functions. In this regard, J scales the deformation and process zone and Q scales the stress triaxiality ahead of the crack tip. In finite geometries, O'Dowd and Shih described the crack tip stress fields as

$$\frac{\sigma_{ij}}{\sigma_o} = \left(\frac{J}{a\,\varepsilon_o\,\sigma_o \ln r}\right)^{1/n+1} \sigma_{ij}(n,\theta) + Q\left(\frac{r\sigma_o}{J}\right)^q \sigma_{ij}(n,\theta) \tag{3}$$

where the first term is the HRR stress field (Hutchinson, 1968a,b) and the second term depends on Q. Based on finite element analysis, they were able to observe in the forward sector ($\theta < 90^\circ$) that the magnitude of the shear stress component is negligible and that the hoop and radial stress components are approximately equal for material with strain hardening coefficient $n > 4$. Based on these observations, eqn (3) can be simplified to

$$\frac{\sigma_{ij}}{\sigma_o} = \left(\frac{J}{a\,\varepsilon_o\,\sigma_o \ln r}\right)^{1/n+1} \sigma_{ij}(n,\theta) + Q\,\delta_{ij}, \tag{4}$$

where δ_{ij} is the Kronecker delta. It is important to notice that Q, which represents a measure of the hydrostatic stress field, is independent of the radial distance r from the crack tip. However, it was shown that for some geometries, Q loses its independence as deformation increases beyond the well contained limit. Alternatively, another way of representing the crack tip stress fields is in terms of the well known small scale yielding solution (SSY). Accordingly, eqn (3) becomes

$$\sigma_{ij} = (\sigma_{ij})_{SSY} + Q\,\sigma_o\,\delta_{ij}. \tag{5}$$

The advantage of this representation is mainly to maintain a radial independence of Q as deformation progresses from well contained to large scale conditions. The Q parameter

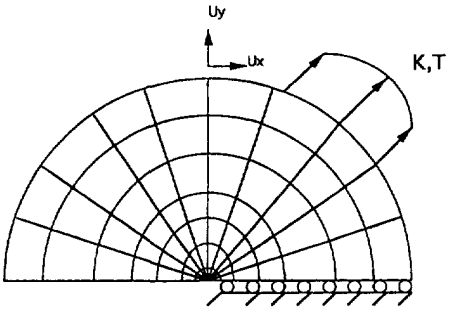

Fig. 6. Schematic of the modified boundary layer formulation (MBL), based on a half-model.

is usually evaluated at a distance of $(r/[J/\sigma_0] = 2)$ which corresponds to the intersection of the finite strain and HRR solutions, right after the blunted zone (McMeeking and Parks, 1979). Other locations where Q could be evaluated along the radial direction are also possible as long as the notations are consistent. This is simply true because Q is independent of the radial distance from the crack tip.

The so-called small scale yielding (SSY) solution can be obtained from a modified boundary layer analysis (MBL) (Betegon and Hancock, 1991). The main objective of the MBL is to obtain geometry independent SSY reference fields. Under SSY conditions, the crack tip fields are self similar and represent the overall response of the structure. In a two-dimensional plane strain analysis, the MBL consists of a semi-infinite edge crack in an infinite circular medium (Fig. 6), loaded remotely by the K field and the transverse stress component T stress

$$\sigma_{ij} = \frac{K_I}{\sqrt{2\pi r}} f_{ij}(\theta) + T\delta_{1i}\delta_{1j}. \tag{6}$$

These are the first two terms of William's expansion of the crack tip linear elastic solution (Williams, 1957). In the present analysis the SSY solution is obtained with the first term only ($T = 0$). Conditions of SSY are satisfied only when the crack tip plastic zone is much smaller than any other dimensions, mainly the crack length. In cases considered in this paper, the crack tip plastic zone is well within the K dominated zone. For further details on the finite element solution, readers are referred to the NCEMT-Interim Report I (1991).

6. FRACTURE TOUGHNESS MEASUREMENT

As mentioned earlier, within the scope of the (J, Q) approach, at increased loading, both the crack driving force J and the crack tip constraint Q are calculated from a two-dimensional plane strain finite element analysis. Collection of these data points form J,Q trajectories which define the evolution of crack tip deformations at the corresponding constraints. Similarly, by testing small laboratory specimens (ASTM-E813, see the Appendix), a (J_{crit}, Q_{crit}) trajectory, called a fracture toughness locus, can be established. It should be pointed out that only the J_{crit} data are measured experimentally. The corresponding Q_{crit} values are computed from the finite element analysis of specimens with identical dimensions, boundary conditions, material properties and applied loads to those used in the ASTM-E813 fracture toughness test. When superimposing the fracture toughness locus on other (J, Q) trajectories that correspond to different crack depths, the intersection of these curves represents a crack initiation data point. The ensemble of these points represents a fracture envelope.

7. RESULTS AND DISCUSSION

Static results

Figure 7 shows that applied pressure increases linearly with respect to the nominal peak strain for base plate (HY-100), weld metal (HY-80) and weldment (HY-100/HY-80)

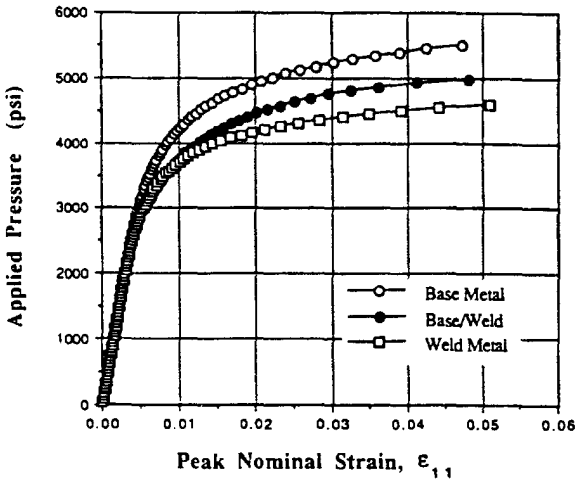

Fig. 7. Static results for uncracked HTEs in terms of applied load versus nominal strain distribution.

specimens up to 0.5% strain. Moreover, the weld metal and base/weld specimens continue to exhibit similar flow behaviour up to about 1% peak strain. Beyond that, each specimen shows a distinct behaviour. As expected, at higher peak strains, the curve for the base/weld specimen falls between the base metal and the weld metal specimens. These results indicate that up to 1% peak strain, plastic yielding in the base/weld specimen is totally confined within the weld zone. Thus, the material behaves similarly to the weld metal specimen. Further increases in the peak strain are accompanied by the plastic yielding in the base metal, which results in the shift of the base/weld curve toward the base plate. It follows that for a similar weld geometry, larger weld volume would introduce a load–peak strain curve that bears a stronger resemblance to the one of the weld metal specimen at higher strains.

Results of the J-integral versus applied pressure for the three materials are shown in Figs 8(a–c). For deep crack specimens, relatively high J-integrals are obtained at low peak strains. Such findings are consistent for all the three material systems. In contrast, shallow crack specimens are characterized by low to moderate J values at high peak strains. They indicated that, as the cracks become deeper, the J-integral tends to increase more rapidly as the pressure increases. Such dramatic differences between shallow and deep cracks imply that the former can sustain higher load with moderate crack driving force (J) while for the latter, J could increase exponentially if the applied load exceeds a threshold value. Some of the numerical results for the static analyses are listed in Table 1.

In all the cases, the J-integral for various crack lengths in each material system is determined by the corresponding material properties and geometrical constraints. For $a/w = 0.025$, a 3% peak strain in the HY-100 system [Fig. 8(a)] corresponds to a J of approximately 2500 in-lb/in^2. Note that this J value is below the bracket of fracture toughness for deep cracked HY-100 material test specimen. In contrast, a much higher J, which is beyond the fracture toughness of both HY-100 and HY-80 test specimen, is obtained for the HY-100/HY-80 system [Fig. 8(c)]. This striking finding can be attributed to factors, such as material mismatch and weld geometry, which ultimately control the crack driving force near the tip. Furthermore, for a given peak strain, the fact that J is lower for the HY-100/HY-80 than that for the HY-100 at other larger crack depths can be readily understood from the mathematical derivation of J. The J-integral introduced by Rice (1968), is proportional to the area under the stress–strain curve. That is to say that for the same crack depth under the same elastic/plastic strain conditions, the near-tip strain fields for HY-100/HY-80 are significantly higher than those of HY-100. It suggests that an undermatched weld inherently exhibits lower fracture resistance than the single base material in static loading conditions.

Figures 9–10 exhibit the progress of plasticity as a function of nominal peak strain. For the HTE with a deep crack ($a/w = 0.25$), plastic yielding was first observed at the

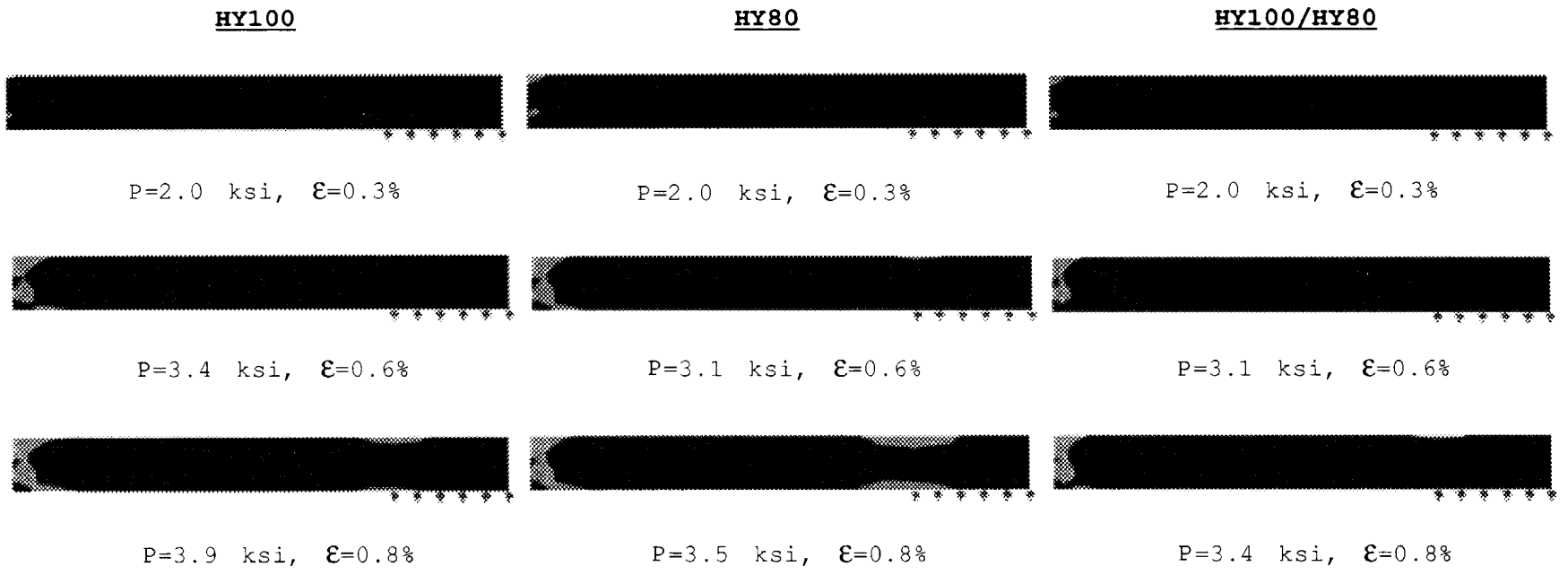

Fig. 9. Evolution of plastic deformation in the HTE with deep cracks under static loads ($a/w = 0.025$).

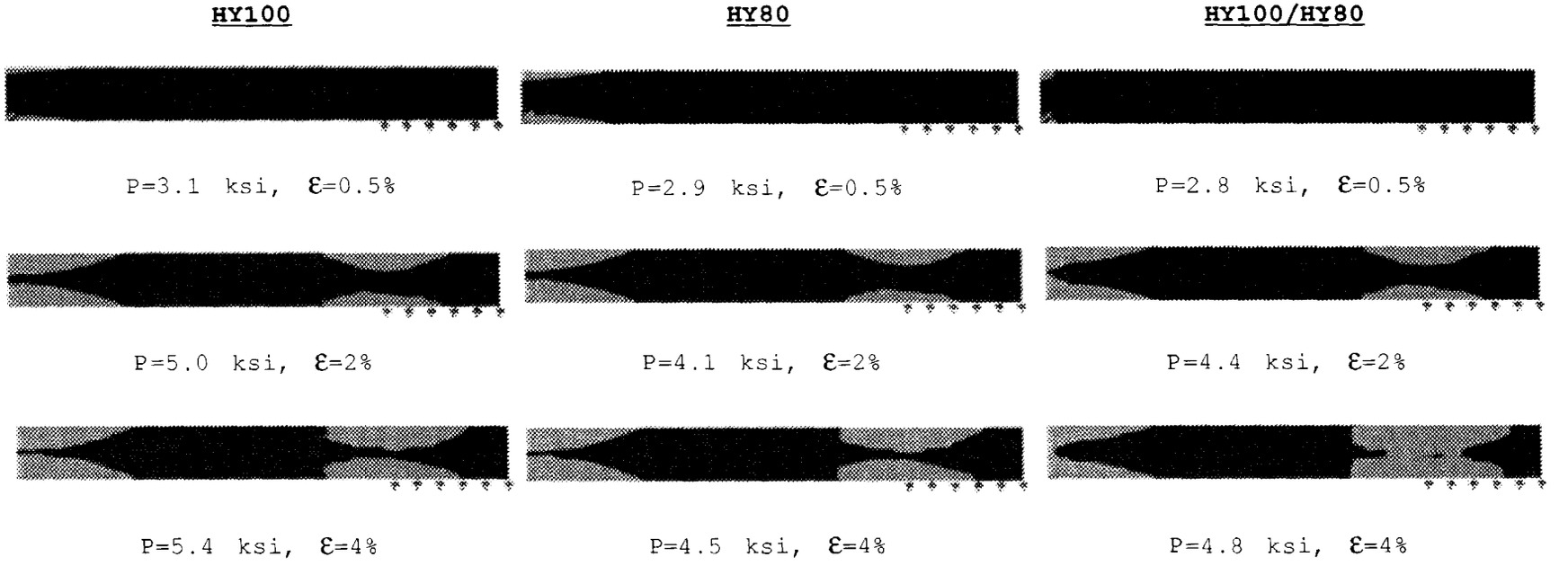

Fig. 10. Evolution of plastic deformation in the HTF with shallow cracks under static loads ($a/w = 0.025$).

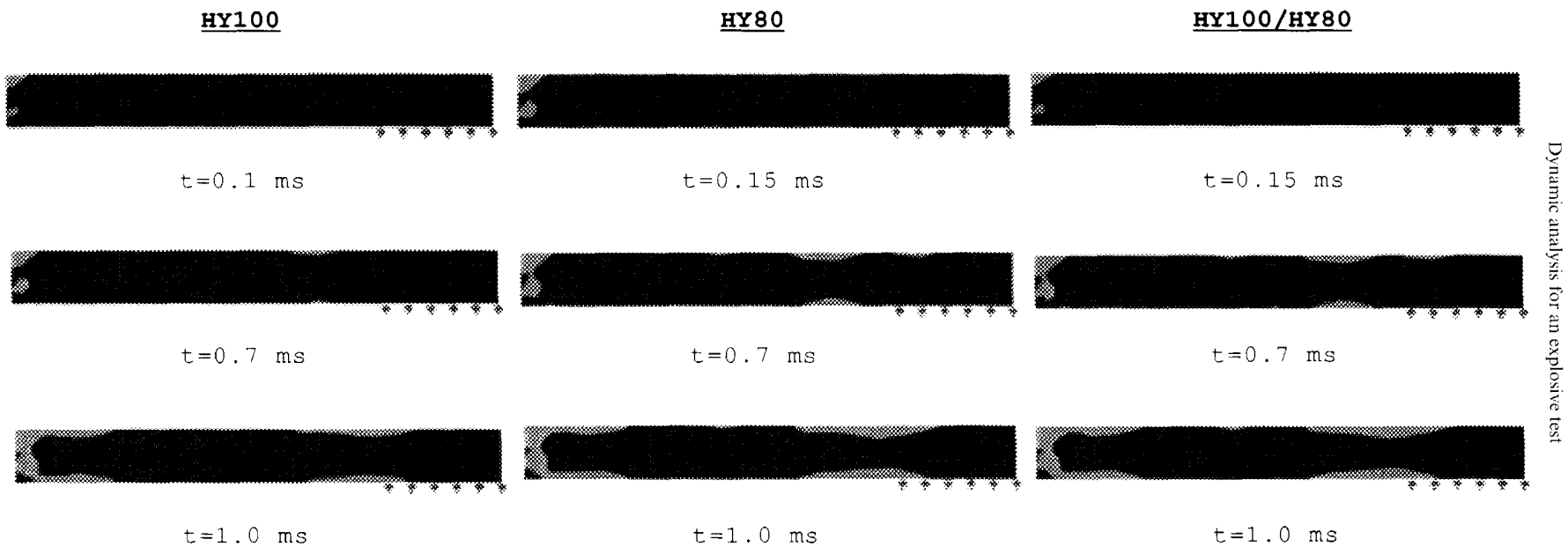

Fig. 15. Evolution of plastic deformation in the HTE with deep cracks under dynamic loads ($a/w = 0.25$).

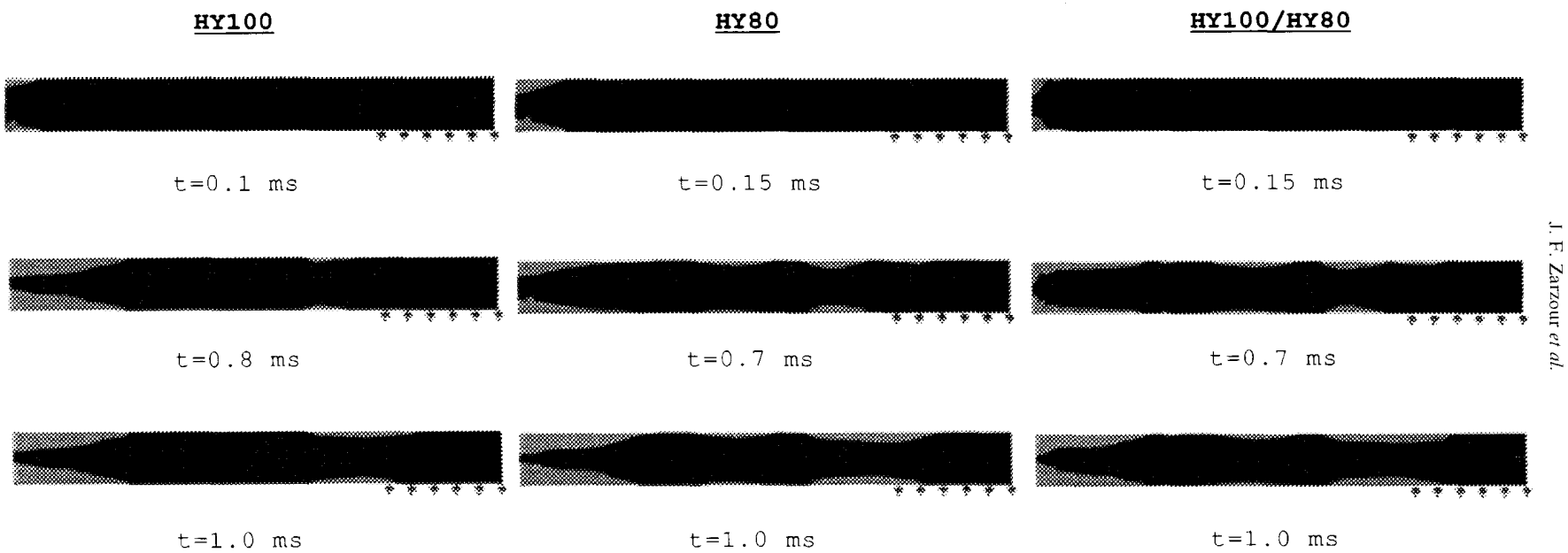

Fig. 16. Evolution of plastic deformation in the HTE with shallow cracks under dynamic loads ($a/w = 0.025$).

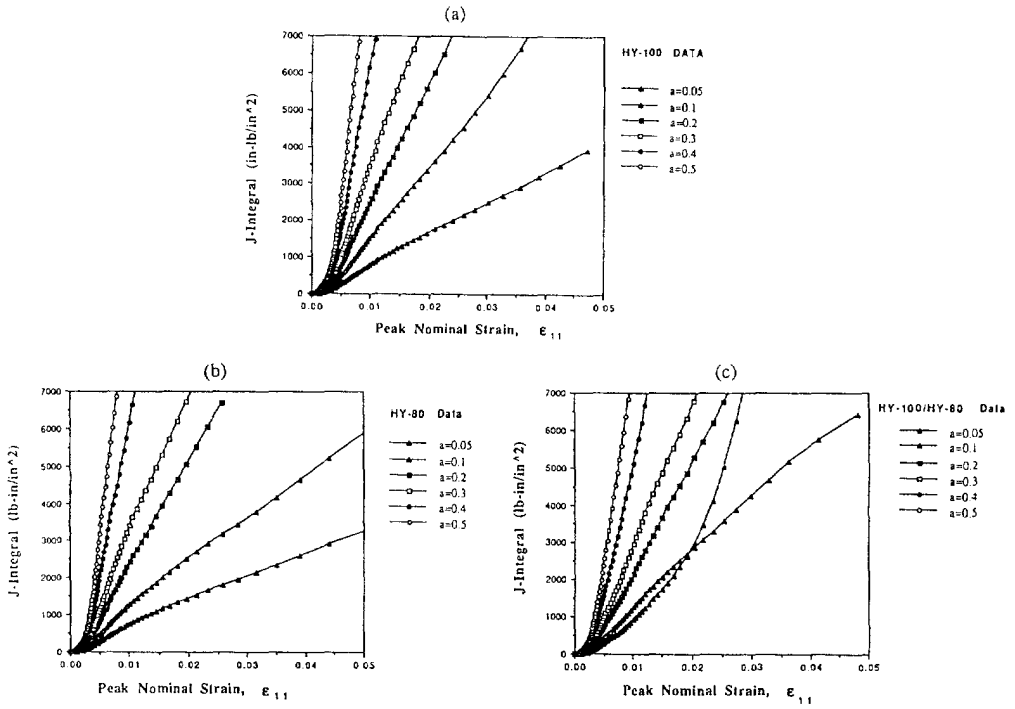

Fig. 8. Static results for cracked HTEs in terms of the J-integral versus peak nominal strain distribution.

region near the crack tip. It follows the extension of the plastic zone to the top surface at a moderate pressure. At the final stage, plastic hinges were developed at the mid-section of the beam and localized deformation was observed at areas close to the spring supports. Similar observations were also made for weld metal and base/weld specimens at three different nominal strains. However, the plastic zone evolves differently for the specimens

Table 1. Static J-integral computations for hull toughness elements (HTE)

Crack depth (in)	HY-100 P (psi)	HY-100 % ε	HY-100 J (in-lb/in^2)	HY-80 P (psi)	HY-80 % ε	HY-80 J (in-lb/in^2)	60° double-V weld HY-100/HY-80 P (psi)	60° double-V weld HY-100/HY-80 % ε	60° double-V weld HY-100/HY-80 J (in-lb/in^2)
	3740	0.931	503	3389	1.005	505	3277	0.644	505
0.05	4840	2.335	1537	4214	2.496	1541	4068	1.171	1465
	5225	3.338	2476	4488	3.912	2602	4407	1.525	2621
	5445	4.452	3499	4580	4.969	3311	4520	1.672	3451
	3190	0.642	522	3023	0.699	528	2994	0.521	519
0.1	4180	1.339	1493	3847	1.679	1556	3898	1.029	1512
	4620	1.949	2401	4168	2.367	2497	4350	1.458	2508
	4950	2.563	3603	4351	3.018	3438	4633	1.835	3565
	2695	0.476	510	2565	0.484	520	2542	0.388	505
0.2	3740	0.931	1536	3343	0.958	1482	3446	0.735	1537
	4180	1.339	2454	3756	1.529	2595	3842	0.986	2458
	4510	1.778	3502	3939	1.844	3388	4124	1.222	3410
	2420	0.415	509	2336	0.419	513	2373	0.352	535
0.3	3465	0.758	1552	3114	0.754	1514	3220	0.617	1581
	3905	1.057	2571	3481	1.116	2526	3616	0.836	2580
	4180	1.339	3464	3710	1.456	3403	3898	1.029	3574
	2090	0.349	519	2015	0.336	511	2034	0.297	521
0.4	3025	0.575	1540	2748	0.560	1537	2825	0.462	1563
	3410	0.731	2513	3069	0.726	2522	3164	0.591	2518
	3685	0.890	3512	3298	0.911	3503	3390	0.704	3389
	1870	0.312	526	1832	0.306	534	1808	0.264	514
0.5	2750	0.488	1584	2473	0.456	1494	2542	0.388	1524
	3080	0.598	2482	2794	0.583	2563	2882	0.480	2572
	3355	0.709	3576	2977	0.673	3417	3051	0.543	3319

with a shallow crack. Figure 10 clearly illustrates that the plastic deformation extends along the top and bottom surfaces without the development of hinges. Nevertheless, the base/weld specimen with a shallow crack shows extensive deformation across the beam thickness at areas close to the mid-section and springs at comparable 4% strain. Such an observation is consistent with the results in Fig. 10 where the energy absorbed for $a = 0.05$ in is significantly higher than the counterparts in Fig. 9.

Dynamic results

As mentioned before, the (J, Q) approach was chosen primarily to cope with the problem of low constraint encountered in the HTE analysis. Analyses were performed on the following material systems: HY-100; HY115; HY-100/HY-80. Prior to computing J, a brief inspection of the relative vertical displacement of some HTEs was made. As shown in Fig. 11(a), the displacement of the beam relative to the undisplaced configuration varies

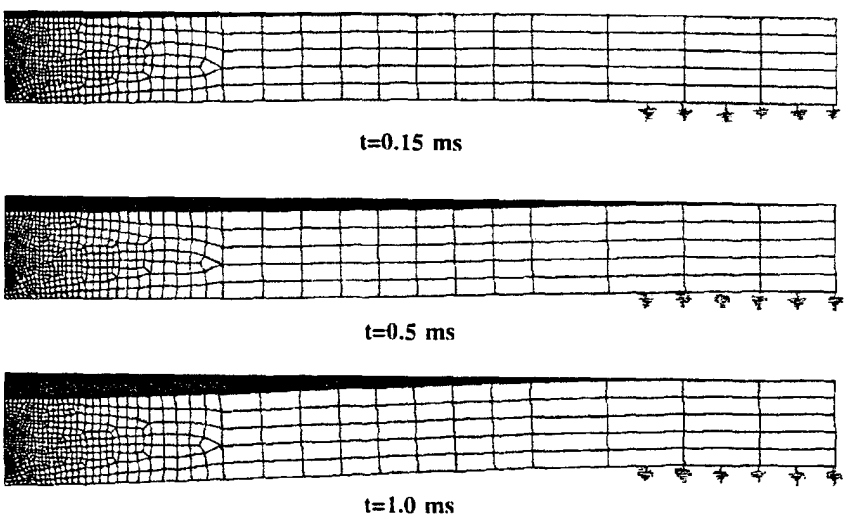

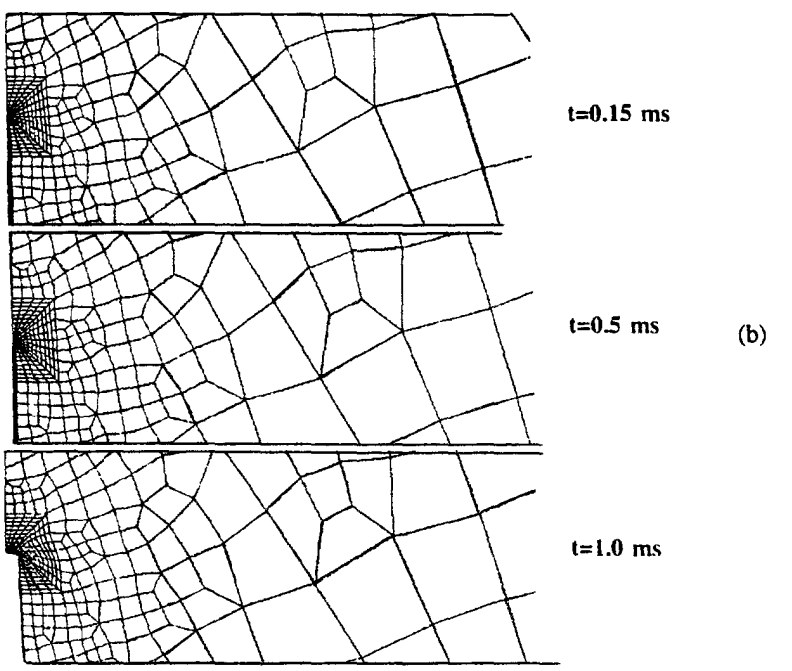

Fig. 11. (a). Progress of relative element displacement under dynamic load: (b) progress of crack tip deformation under dynamic load (10x).

from about 10% at 0.15 ms to about 40% at 1.0 ms. For the same time intervals, the corresponding crack tip geometries (with 100% magnification) for a deep cracked HTE ($a/w = 0.25$) are indicated by Fig. 11(b). For the purpose of comparing CTOD to J, which is valid for static loading conditions, some limited calculations of CTODs were carried out using the method of 90° intercept proposed by Rice (1968).

For cracked elements, the evolution of the J-integral as a function of time is shown in Figs 12(a–f) and 13(a–f). Within the specimens, initial linear elastic stress wave fronts can be expected. Therefore, stress is linearly proportional to time. After the interaction with the crack, a time-dependent J-integral is developed. This consideration would apply to the first longitudinal stress wave front. Its influence, however, is very small and only small J values are calculated [see J at times $t < 0.1$ ms in Figs 12(a–f) and 13(a–f)]. Similar observations were made by an early work of Ahmad *et al.* (1983). They indicated that in their impact tests, the first significant increase in crack tip loading occurred only for times

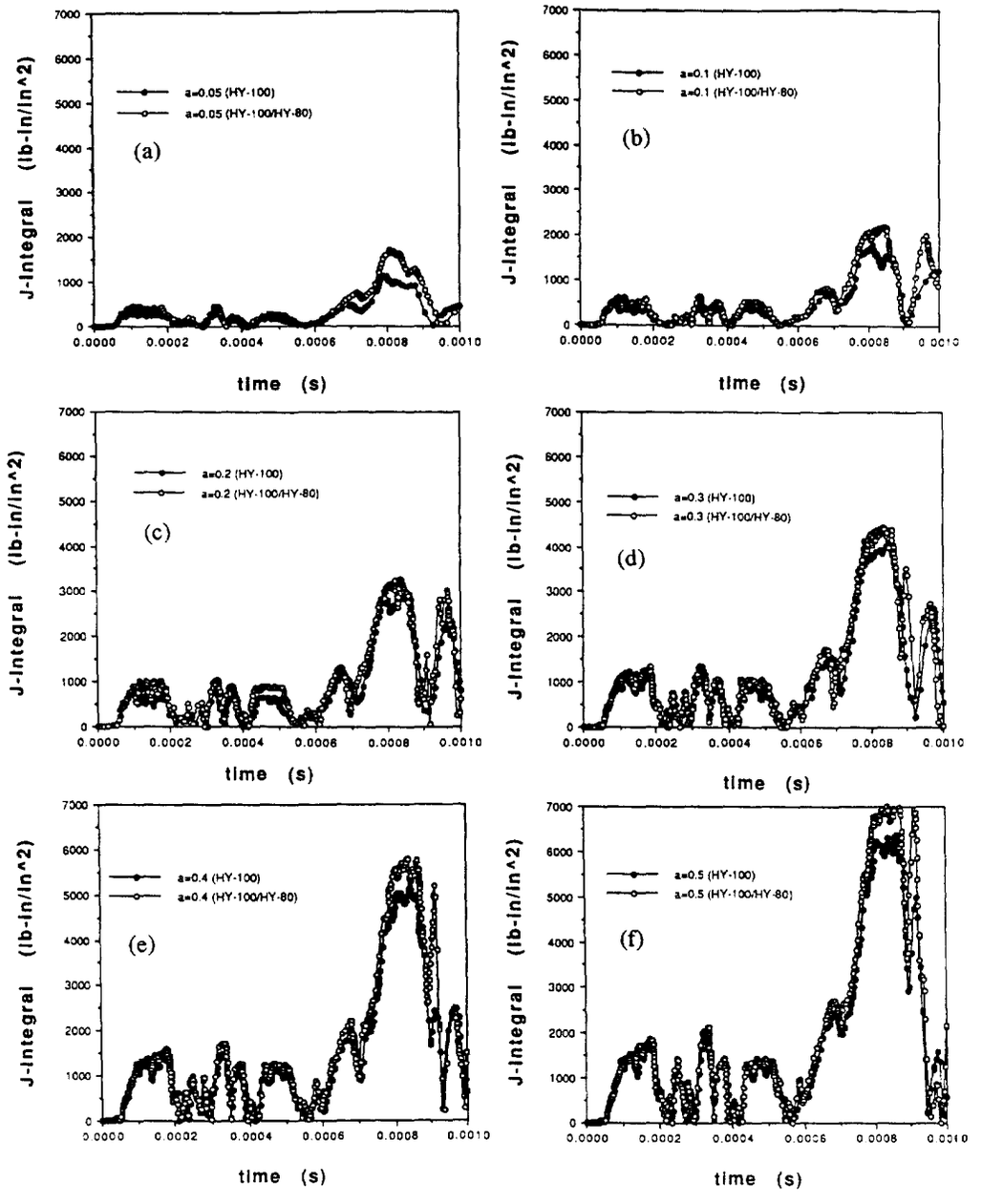

Fig. 12. Prediction of J for cracked HY-100 and HY-100/HY-80 HTEs with different crack sizes.

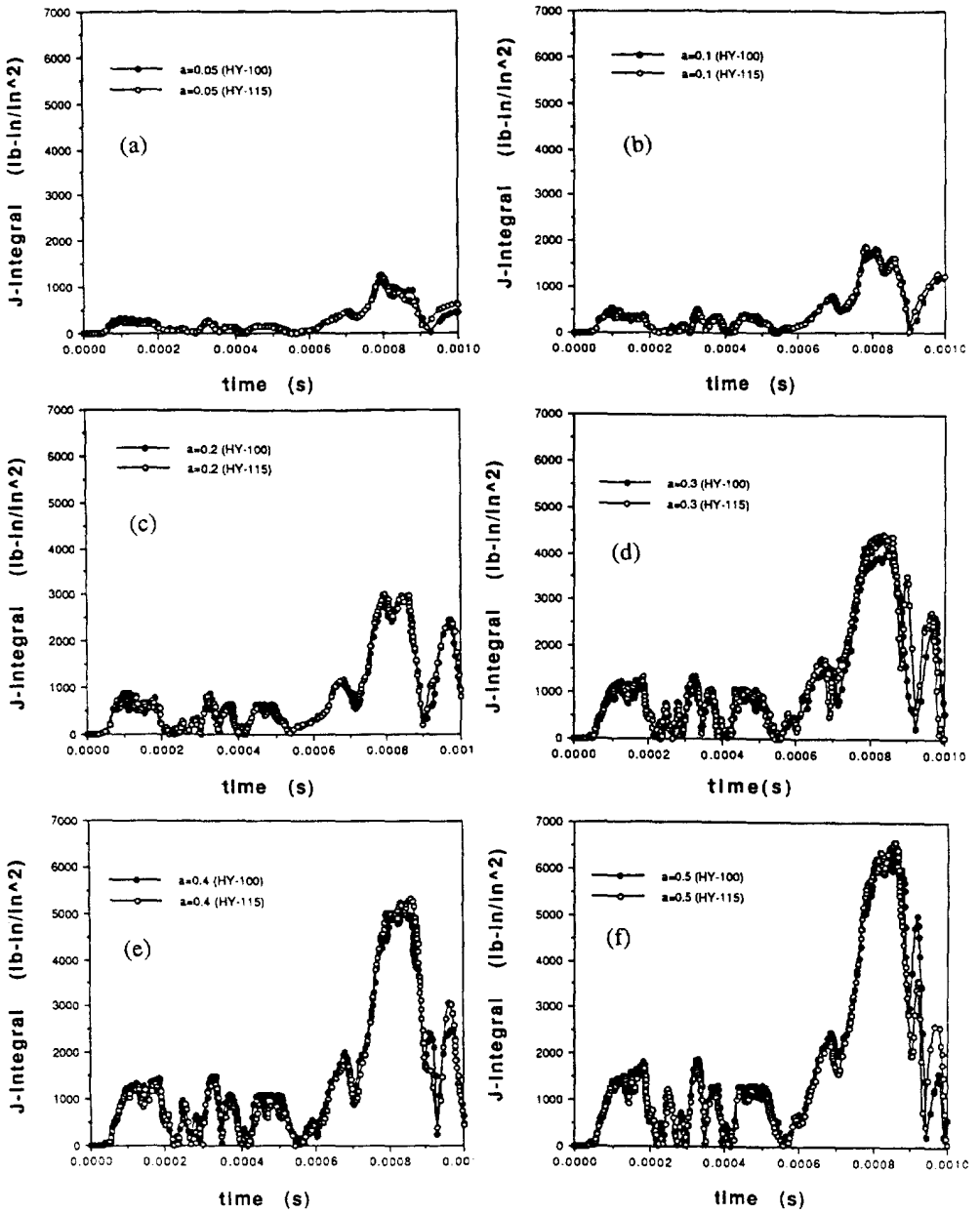

Fig. 13. Prediction of J for cracked HY-100 and HY-115 HTEs with different crack sizes.

comparable to the arrival of the transverse wave front excited at the impact point. In the present analyses, peak values of J were invariably observed in the vicinity of 0.8 ms for all the cases studied. By comparing the J versus time diagrams for the HY-100 and HY-100/HY-80 systems [Figs 12(a–f)], the following are noted: (a) qualitatively similar J-integral histories were observed; (b) all J_{max}s occur at approximately 0.8 ms for different crack depths; (c) the difference in amplitude of J_{max} increases as crack depth decreases (i.e. for $a = 0.05$ in, $J_{max} = 1500$ lb-in/in^2 and for $a = 0.5$ in, $J_{max} = 6500$ lb-in/in^2). Similar observations were also made in the previous static analyses. It should be pointed out that J_{max} is achieved at the same load amplitude in all models. In Fig. 14, the rate of change in J_{max} at the corresponding time is obtained for both HY-100 and HY-100/HY-80 systems. These results clearly display the substantial differences between the two material systems at all crack depths. In contrast, a comparison between HY-115 and HY-100 systems [Figs 13(a–f)] indicates that the discrepancies between the corresponding J–time diagrams at

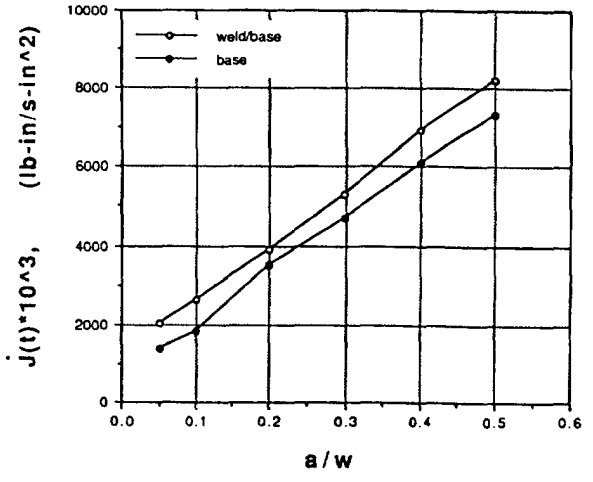

Fig. 14. Difference in the rate of J ($J(t) = J_{max}/t_{max}$) between HY-100 and HY-100/HY-80 HTEs.

identical crack lengths are negligible. Therefore, it is concluded that the material hardening behavior does not significantly affect the crack driving force J.

The plasticity evolutions under dynamic loading for different crack lengths are illustrated in Figs 15–16. For a HY-100 element with a deep crack ($a/w = 0.25$), the specimen is elastic everywhere at time below 0.1 ms. As time increases to 0.1 ms, plasticity starts to develop concurrently at the crack tip and the top surface of the mid-section of the beam (below the applied load). At time equal to 0.8 ms, localized plasticity is also observed at locations remote from the crack tip right next to the elastic springs. This progress continues up to 1.0 ms where plastic hinges form in the ligament and extends along the top and bottom surfaces of the element. Similar trends can be seen in the weld metal and base/weld material systems. However, for a HY-100 specimen with a shallow crack ($a/w = 0.025$), plasticity appeared initially at the crack tip and then extended back to the free surfaces. At the same time, plastic yielding was also observed at the top mid-section. At time equal to 1.0 ms, plasticity evolves along the top and bottom surfaces as well as locations adjacent to the elastic springs. However, the central part of the ligament remains elastic.

The stress fields near the crack tip, especially the opening mode components, were investigated in great detail. In Figs 17(a–f) through Figs 19(a–f), normalized stress components, σ_{11}/σ_o, are plotted against the normalized distance ahead of the crack tip, $r/(J/\sigma_o)$, where σ_{11} was determined based on selected J values along the J–time diagrams. Since the analyses focus on the opening of the crack tip, all Js were selected at values not beyond the J_{max}. In addition, a curve representing the reference stress field, which characterized a small scale yielding (SSY) solution for the particular material system, was also shown. The SSY reference field represents the highest normalized stress components attainable under high constraint conditions. A common trend in these results is that as load increases (or $r/(J/\sigma_o)$ decreases), normal stresses tend to approach the SSY fields. However, as crack depth decreases (i.e. low constraint), gaps between the individual normal stress component and the SSY (at the same load) become wider. This characteristic is found to be more pronounced for the HY-100/HY-80 than for the single material system. It is worth mentioning that deviation from the SSY occurs at times well before the element reaches the peak nominal strain.

A final set of results are expressed with J and the corresponding constraint parameter Q. Q was computed at $r/(J/\sigma_o) = 2$ which falls on the borderline dividing small strain and finite strain theories. Again, results are obtained for the three material systems. Figure 20 illustrates the six J vs Q trajectories that represent each crack depth. Based on the guidelines of the (J, Q) approach, negative Q values indicate low crack tip stress triaxiality (low constraint or low hydrostatic stress) while positive Q values indicate high crack tip constraint. Q equal to zero corresponds to the special case where the crack tip fields are equal to the SSY distribution. A deep crack generates a crack driving force that rises steeply with constraint whereas a shallow crack produces a driving force curve with a shallow

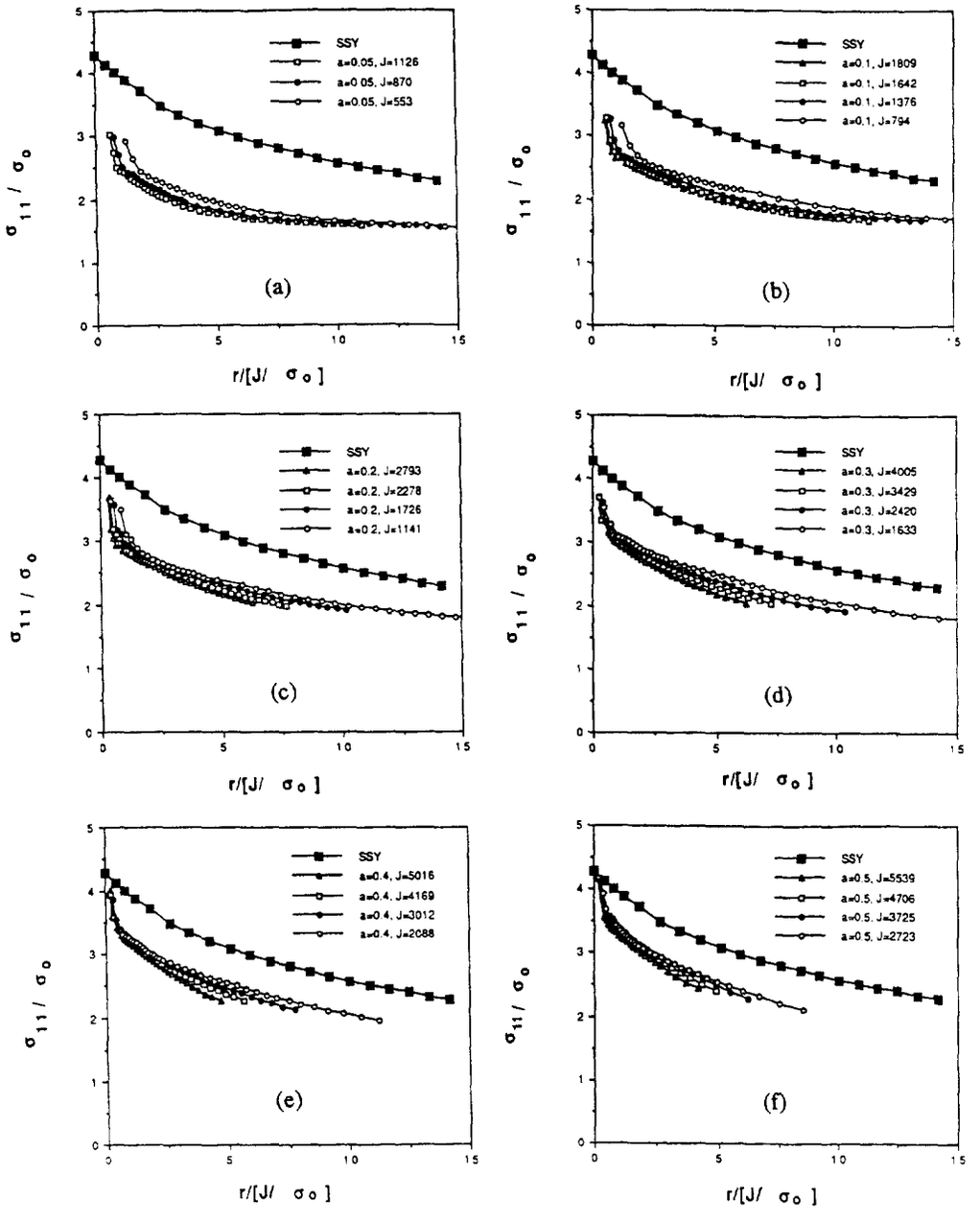

Fig. 17. Normal component of the crack tip stress field obtained at different applied loads (a = 0.05–0.5 in, HY-100).

slope. The final crack initiation prediction, as characterized by J and Q, will be obtained after superposition of the experimental fracture locus (see the Appendix). This is discussed in detail in the next section.

J–Q *Predictions*

The fracture toughness locus of HY-100 is incorporated into the J–Q trajectories as shown in Fig. 21(a). This will be used to assess the fracture toughness of the HTE. Because of the experimental scattering in the fracture toughness data (see the Appendix), both fracture toughness loci in Fig. 21(a) correspond to upper and lower bounds. For a given crack depth, intersection of individual J–Q trajectories with the fracture toughness loci represent a crack initiation data point characterized by the crack driving force and crack tip constraint. Figure 21(a) clearly shows that specimens with crack depth below 0.2 in are

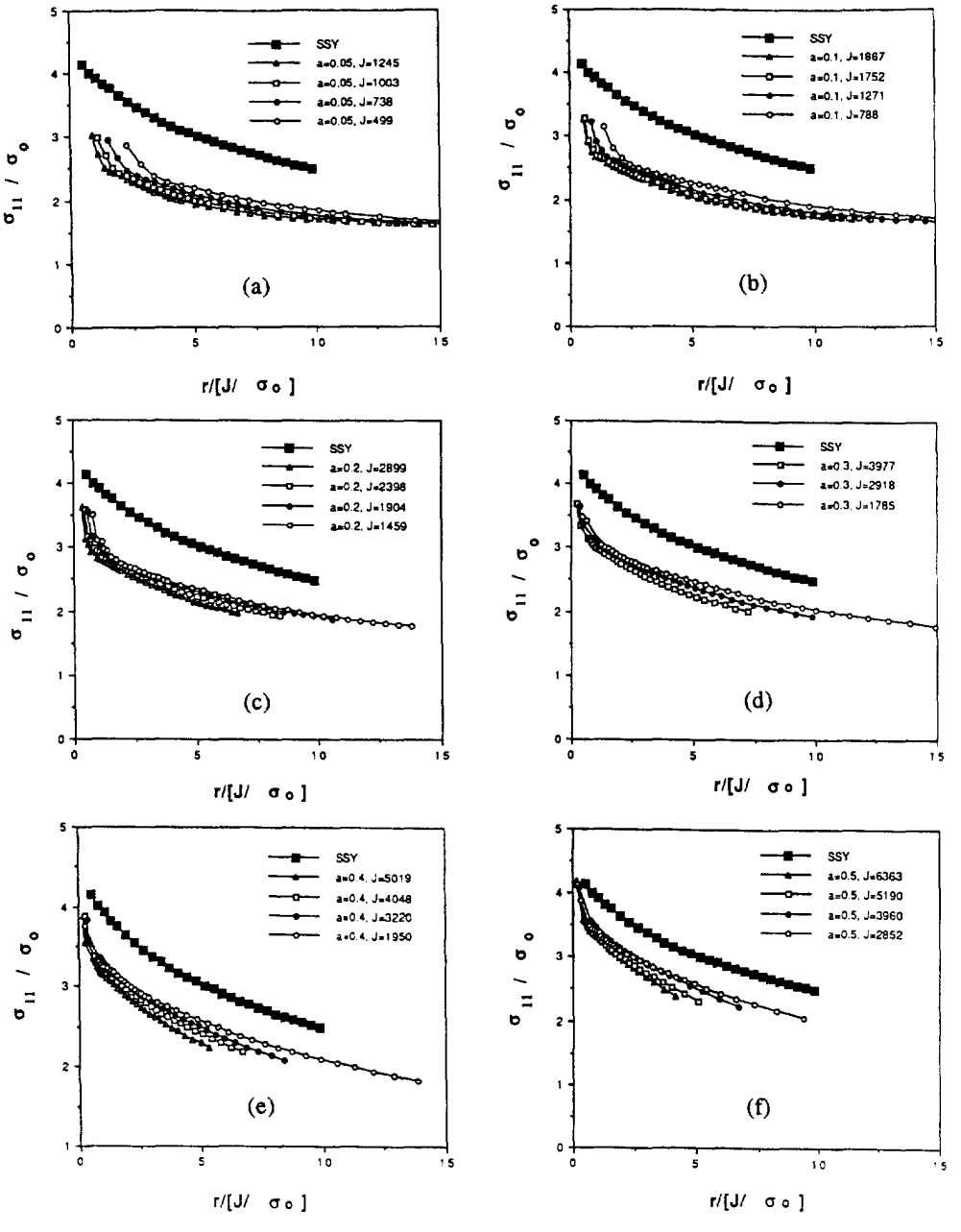

Fig. 18. Normal component of the crack tip stress field obtained at different applied loads (a = 0.05–0.5 in, HY-115).

well below the toughness loci, whereas intersection has already occurred for other crack depths. The implication is that cracks will not initiate for existing shallow cracks ($a < 0.2$ in), while deeper cracks are susceptible to initiation. Also, distances between the (J_{max}, Q_{max}) data point and the fracture toughness loci for each curve indicate a safety bracket. These results appear to correlate well with those observed in earlier experimental programs for HY-100 and HY-80 systems [Fig. 21(b)]. Unlike a single criterion prediction where fracture toughness is designed for rather deep cracks, the present methodology provides a means to couple material property to structural geometry via an additional constraint parameter Q. This can help to accurately predict the fracture behavior of large structures subjected to complex loading conditions where only the crack tip parameters, such as driving force and constraint, need to be computed. However, it should be emphasized that the accuracy of the present scheme is strictly dependent on the success of the experimental fracture data.

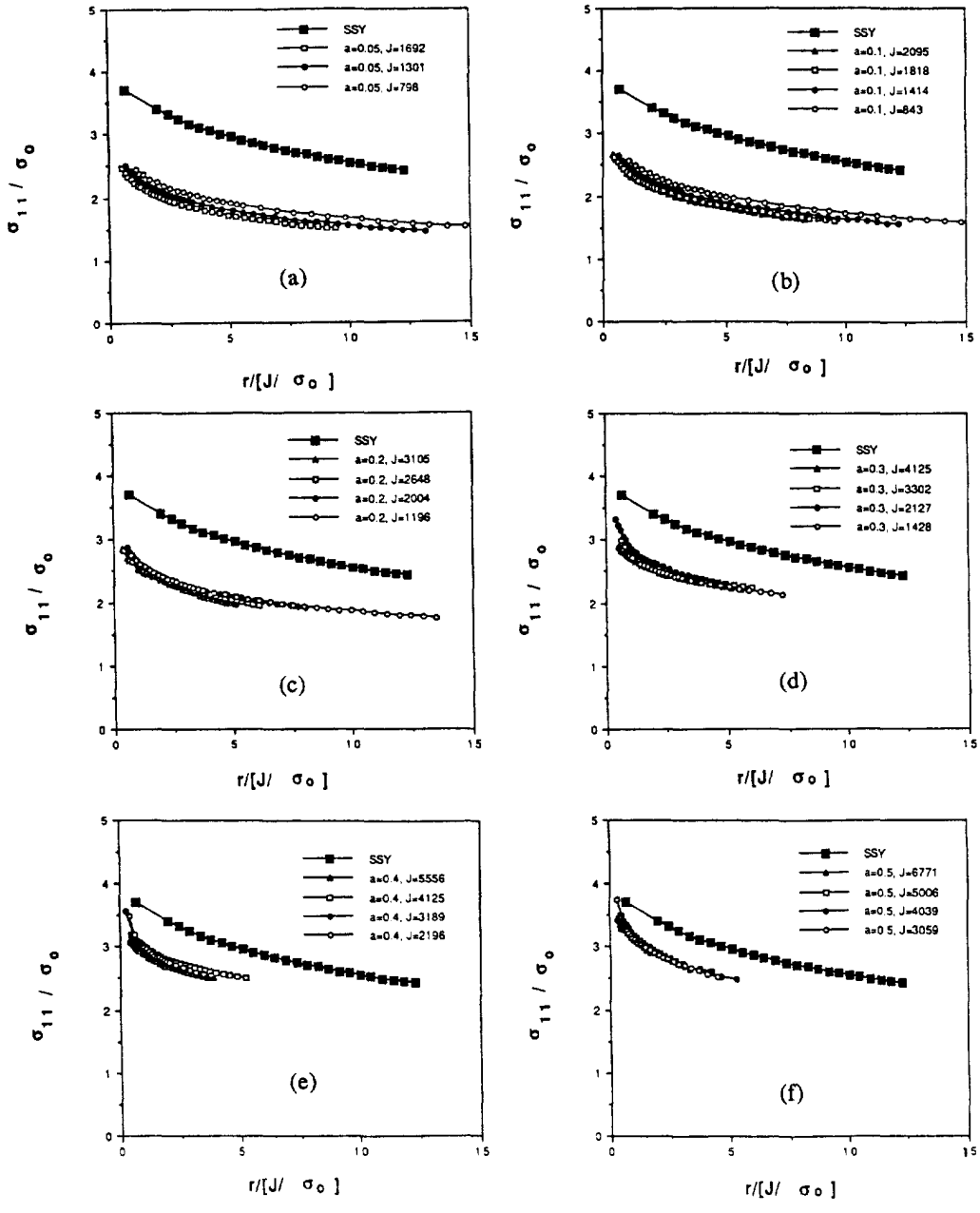

Fig. 19. Normal component of the crack tip stress field obtained at different applied loads ($a = 0.05$–0.5 in, HY-100/HY-80).

In view of the current HTE analysis, it appears that the (J, Q) approach provides the basis for a convenient engineering tool to couple toughness to crack tip constraint. Results of the HTE support the conclusion that the numerical prediction based on the (J, Q) approach can be considered as a first order approximation. Since the actual HTE test is prohibitively expensive, the current prediction can play a versatile role, mainly in providing fracture prediction for new material systems with different toughness. However, it remains to be determined if the actual HY-100/HY-80 material system will provide similar correlations. Testing for fracture toughness on HY-100/HY-80 specimens to construct a fracture toughness loci is considered in the next step of this program. Nevertheless, the (J, Q) approach is proven to be a vital tool for measuring crack initiation at different crack tip constraints.

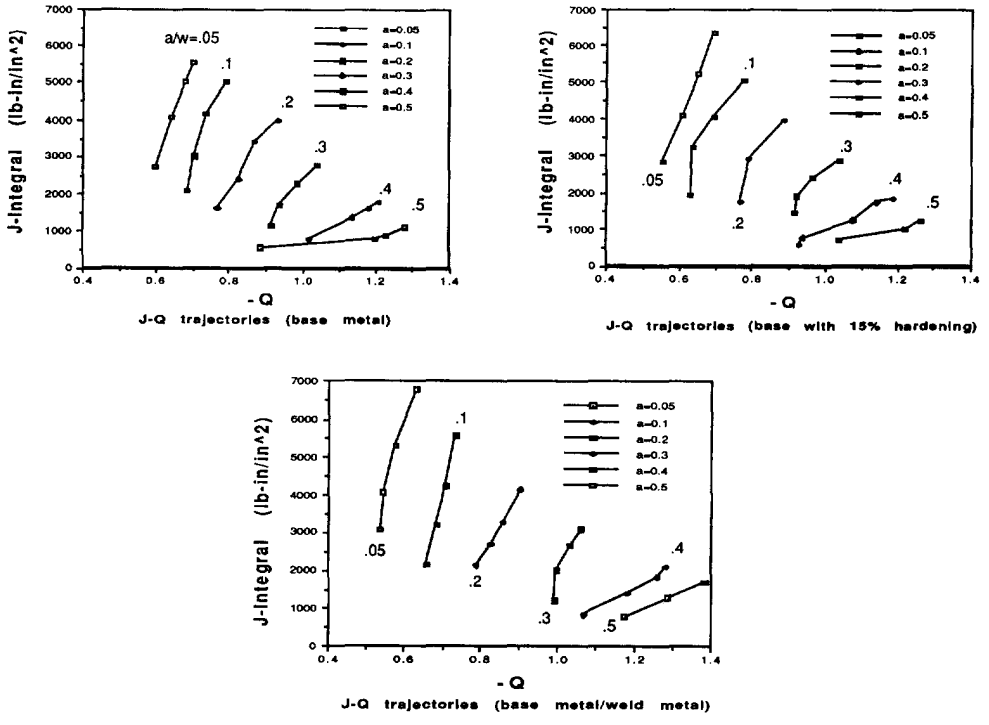

Fig. 20. *J–Q* trajectories for the three material systems at all crack depths.

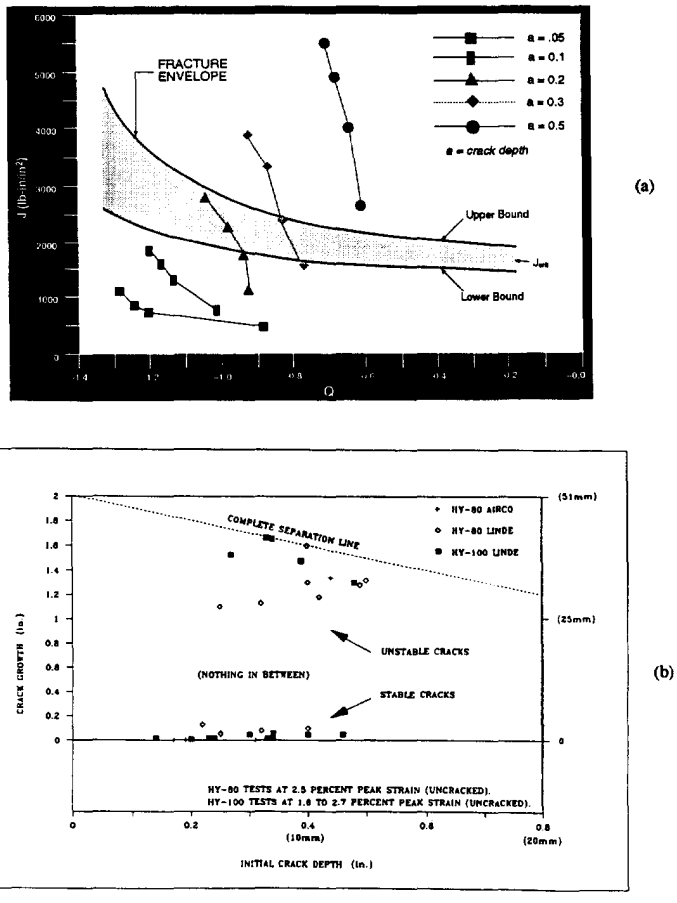

Fig. 21(a). Fracture envelope of the (HTE) as predicted by the (*J–Q*) criterion; (b) crack growth results from HTE tests of 2 in thick welds (after Gifford *et al.* (1990).

8. CONCLUSION

In conclusion, it was demonstrated that the (J, Q) approach can be used effectively in the HTE analysis. This work includes a study of the crack tip fracture environment in terms of the mode I stress field distributions, the J-integral and corresponding constraints measured by the Q parameter. It was demonstrated that the (J, Q) trajectories can be quantified for each material system. These results will then help in deciding about crack initiation in HTEs with different crack depths. To summarize the major findings of the current study, the following remarks are made.

(1) The effect of weld strength mismatch on the crack driving force appears to be insignificant. On the other hand, the impact of HY-100 on J is quite significant for HTEs with shallow cracks ($a/w = 0.025$) and almost non-existent for HTEs with deeper cracks.

(2) The results of the opening mode stress fields indicated that regardless of the crack depth, the stress curves are consistently below the reference stress field obtained in terms of the small scale yielding distribution. Also, for shallow cracks ($a/w = 0.025$), the stress fields are well below the SSY (in the order of σ_0).

(3) At the peak value of J (J_{max}), HTEs with shallow cracks and deep cracks alike exhibited large scale yielding distributions. Plastic hinges are developed across the ligament and through the thickness of these specimens.

(4) The numerical predictions agree remarkably well with those reported in the experimental program. The corresponding failure envelope based on small fracture toughness specimens appears to provide a rigorous terminus for crack driving force curves at a given crack depth.

Acknowledgements—The authors would like to thank Dr F. C. Shih and Mr L. N. Gifford for their valuable advices and comments. This work was conducted by the National Center for Excellence in Metalworking Technology (NCEMT), operated by Concurrent Technologies Corporation, under contract to the United States Navy as part of the United States Navy Manufacturing Technology Program.

REFERENCES

ABAQUS. (1992). User's Manual, Version 5.2. Hibbit, Karlson and Sorensen, Providence, RI.

Ahmad, J., Jung, J., Barnes, C. R. and Kanninen, M. F. (1983). Elastic–plastic finite element analysis of dynamic fracture. *Engng Fract. Mech.* **17**(3), 235–246.

Betegon, C. and Hancock, J. W. (1991). Two-parameter characterization of elastic–plastic crack-tip fields. *ASME J. Appl. Mech.* **58**, 104–110.

Carlberg, J. R., Wiggs, A. J. and Sickles, J. B. (1988). Explosive testing of full thickness precracked weldments. DTRC-SSPD-88-172-42.

Dodds, R., Jr, Shih, C. F. and Anderson, T. L. (1992). Continuum and micromechanics treatment of constraint in fracture. UILU-ENG-92-2014, Civil Engineering Studies, Structural Research Series No. 573, University of Ilinois.

Elliott, D. M., Caudrey, A. J. and Sumpter, J. D. G. (1987). Standard procedure for underwater flawed bulge explosion (FBE) testing; with Appendix by F. Livingstone. ARE TM (USS) 87212.

Gifford, L. N. (1991). Ship structures and protection department research and development report—a snapshot of research in submarine hull toughness. DTRC-SSPD-92-172-7.

Gifford, L. N., Carlberg, J. R., Wiggs, A. J. and Sickles, J. B. (1990). Explosive testing of full thickness precracked weldments. ASTM-STP 1074, *Fract. Mech. 21st Symp.* (Edited by J. P. Gudas, J. A. Joyce and E. M. Hackett), pp. 157–177. American Society for Testing and Materials, Philadelphia, PA.

Hilber, H. M. and Hughes, T. J. R. (1978). Collocation, dissipation and "overshoot" for time integration schemes in structural dynamics. *Earthquake Engng Struct. Dynamics* **6**, 99–117.

Hutchinson, J. W. (1968a). Singular behavior at the end of a tensile crack in a hardening material. *J. Mech. Phys. Solids* **16**, 13–31.

Hutchinson, J. W. (1968b). Plastic stress and strain fields at a crack tip. *J. Mech. Phys. Solids* **16**, 337–347.

McMeeking, R. M. and Parks, D. M. (1979). On criteria for J-dominance of crack-tip fields in large scale yielding. In *Elastic–Plastic Fracture Mechanics*, pp. 175–194. ASTM-STP 668, Philadelphia, PA.

Nakamura, T. (1987). Computational methods and results for dynamic fracture. Ph.D. Thesis, Division of Engineering, Brown University.

Nakamura, T., Shih, C. F. and Freund, L. B. (1985). Analysis of a dynamically loaded three-point-bend ductile fracture specimens. Brown University Report ONR0365/1.

NCEMT-Interim Report I. (1991). Optimized weldment properties for full-penetration butt welds in HY-100 steel submarine structures program, phase II—joint strength and structural determination.

O'Dowd, N. P. and Shih, F. C. (1991). Family of crack-tip fields characterized by triaxiality parameter. Part I—Structure of fields. *J. Mech. Phys. Solids* **39**(8), 989–1015.

O'Dowd, N. P. and Shih, F. C. (1992). Family of crack-tip fields characterized by triaxiality parameter. Part II—Fracture applications. *J. Mech. Phys. Solids* **40**, 939–963.

Parks, D. M. and Wang, Y. Y. (1988). Elastic–plastic analysis of part-through surface cracks. *Proc. ASME Symp. Three-dimensional Effects Fract.* ASME, New York.
Porter, J. F. (1991). DREA explosion testing program. 3rd CF/CRAD Meeting on Research in Fabrication and Inspection of Submarine Pressure Hull.
Porter, J. F., Morehouse, D. O. and Matthews, J. R. (1988). Response of SMA and narrow gap weldments to explosive shock loading. Technical Memorandum 88/206, Defense Research Establishment, Atlantic Dockyard Laboratory.
Puzak, P. P. and Pellini, W. S. (1961). Standard evaluation procedures for explosion bulge testing (weldments). NRL Memorandum Report 1255.
Rice, J. R. (1968). A path independent integral and the approximate analysis for strain concentration by notches and cracks. *ASME J. Appl. Mech.* **35,** 379–386.
Ritter, J. C. and Dixon, B. F. (1985). Explosive bulge testing of Australian HY-80 steel plate. Department of Defense Report MRL-R-958, Melbourne, Victoria, Australia.
Sickles, J. B. and Daily, J. W. (1991). Dynamic test methods for certifying fracture resistance of steel and welding procedures for marine structures. DTRC-SSPD-91-172-72.
Williams, M. L. (1957). On the stress distribution at the base of a stationary crack. *ASME J. Appl. Mech.* **24,** 109–114.

APPENDIX: FRACTURE TOUGHNESS RESULTS

These tests are performed to obtain fracture toughness data for three point bend specimens at various crack length/width ratios (a/w). ASTM-E813, standard test method for J_{Ic}, was used as a guideline for the tests because it is designed to evaluate the crack growth resistance of ductile engineering materials including HY steels. In this program, only base metal (HY-100) was tested. A total of 10 specimens were examined at WMT&R. The test matrix consisted of three specimens with deep cracks ($a/w = 0.5$), three specimens with shallow cracks ($a/w = 0.05$) and two specimens each for both of the intermediate crack depths ($a/w = 0.1$ and 0.3). Specimens were machined in accordance with standard configurations with minor modifications. The dimensions were 2 in wide by 1 in thick, with an 8 in span between the two end supports. All specimens were fatigue precracked using a frequency of 25 H and an R ratio of 0.1. Upon completion of precracking, the specimens were side grooved to a depth equal to 20% of the nominal thickness (10% per side). The specimens were then tested at room temperature (75°F) using an Instron 8500 servo-hydraulic test stand and an automated computer controlled testing procedure.

During the tests, the J-integral is calculated based on the area under the load versus load–line displacement (LLD) curve for a given total deflection. The J value is defined by

$$J_{tol} = J_{el} + J_{pl} = \frac{K_c^2(1-\nu^2)}{E} + \frac{\mu_{pl} U_{pl}}{B(w-a)}, \tag{A1}$$

where U_{pl} is the plastic energy or the area under load versus LLD curve, B, w, and a are thickness, width and crack depth of the specimen, respectively, and μ_{pl} is the plastic etafactor.

Subsequently, J-integral values are plotted against the corresponding measured incremental crack growth values (Δa_p). A linear regression line of the form

$$\ln J = \ln C_1 + C_2 \ln \Delta a_p \tag{A2}$$

can thus be obtained using a method of least squares. Also, a blunting line with the slope equal to twice the effective yield strength (σ_y) is plotted. A separate line, parallel to this blunting line and intersecting the abscissa at 0.008 in (0.2 mm), is drawn. The intersection point of the second line and the regression curve is designated as J_Q and Δa_Q. When testing conditions meet the validity requirements per ASTM-E813, then J_Q is said to be equivalent to J_{Ic}, otherwise J_Q will be referred as J_{crit}.

Table A1 summarizes the test results. Only the deep cracked specimens ($a/w = 0.5$) have been complied with the validity criteria per ASTM-E813. In general, a linear relationship between the load and the load–line displacement was first observed and followed by a highly nonlinear path until the specimen fractured. The range of such nonlinearity increases as the crack depths become smaller. The later sections will show how these data are used to derive the Q stress fields for structures of different crack lengths. The resulting J–Q fracture toughness locus will be used to define the fracture envelope for the materials tested.

Table A1. HY-100 shallow crack fracture toughness test data

Specimen number	Temperature (°F)	S (in)	B (in)	W (in)	a(in)	a/W	CTOD (in)	J_{Ic} (J_Q) (in-lb/in^2)	K_{Ic} (K_{IQ}) from J ksi (in)$^{1/2}$	P_Q (kpsi)	P_{max} (kpsi)
1	75	8	1	2	1.1515	0.5757	0.018	1617.05	220.25	7.800	12.121
2	75	8	1	2	1.1907	0.5953	0.028	1754.90	229.45	7.840	11.170
3	75	8	1	2	1.2006	0.6003	0.027	1643.88	222.07	7.840	10.891
4	75	8	1	2	0.6285	0.3139	0.036	3146.74	307.25	20.470	31.559
5	75	8	1	2	0.6189	0.3095	0.036	2537.57	275.91	28.100	31.008
6	75	8	1	2	0.1936	0.0968	0.016	2623.31	280.53	28.100	52.300
7	75	8	1	2	0.2260	0.1130	0.036	1583.76	217.97	20.900	53.919
8	75	8	1	2	0.1006	0.0503	0.034	2539.38	276.01	28.200	62.063
9	75	8	1	2	0.1115	0.0558	0.034	3149.52	307.39	28.800	60.862
10	75	8	1	2	0.1161	0.0581	0.027	1933.54	240.84	27.200	57.791